arXiv:0707.2279v2 [hep-ex] 13 Nov 2007

Measurement of the $e^+e^- \to K^+K^-$ cross section in the energy range $\sqrt{s} = 1.04$–1.38 GeV with the SND detector at VEPP-2M e^+e^- collider

M. N. Achasov,[1,2] K. I. Beloborodov,[1,2] A. V. Berdyugin,[1,2] A. G. Bogdanchikov,[1]
A. D. Bukin,[1,2] D. A. Bukin,[1] T. V. Dimova,[1,2] V. P. Druzhinin,[1,2]
V. B. Golubev,[1,2] I. A. Koop,[1,2] A. A. Korol,[1] S. V. Koshuba,[1] E. V. Pakhtusova,[1]
E. A. Perevedentsev,[1] S. I. Serednyakov,[1,2] Yu. M. Shatunov,[1,2]
Z. K. Silagadze,[1,2] A. N. Skrinsky,[1] Yu. V. Usov,[1] and A. V. Vasiljev[1,2]

[1]*Budker Institute of Nuclear Physics, Novosibirsk, 630090, Russia*
[2]*Novosibirsk State University, Novosibirsk, 630090, Russia*

The cross section of the process $e^+e^- \to K^+K^-$ was measured in the energy range $\sqrt{s} = 1.04$–1.38 GeV in the SND experiment at the VEPP-2M e^+e^- collider. The measured cross section is described by the model of Vector Meson Dominance with contributions from the light vector mesons ρ, ω, ϕ and their lowest excitations. The mean statistical accuracy of the measurement is 4.4 %, and the systematic uncertainty is 5.2 %.

PACS numbers: 13.66.Bc 14.40.n 12.40.y 13.40.Gp

I. INTRODUCTION

The experimental study of the process $e^+e^- \to K^+K^-$ at energies ≥ 1 GeV is of interest for a number of reasons. First, this is one of the processes in which the excited states of the light vector mesons whose characteristics until now have not been reliably established, should manifest themselves. Second, the cross section of this process is determined by the form factor of charged kaon, whose knowledge together with the data on the neutral kaon form factor, measured in the reaction $e^+e^- \to K_SK_L$ [1] at the same energies, makes possible a calculation of the isovector and isoscalar form factors of kaons and determination of the parameters of the excited states of light vector mesons. Third, the isovector form factor of a kaon obtained in e^+e^- annihilation can be used to test conservation of vector current by using experimental data on the τ lepton decay modes with kaons [2]. And finally, the process production of charged kaon pairs contributes to the total hadron production cross section and its accurate knowledge is interesting for the Standard Model tests, for example, for the measurement of the muon anomalous magnetic moment.

The first observation of pair production of charged kaons in e^+e^- interactions in the energy region above the ϕ meson resonance was performed at Novosibirsk collider VEPP-2 in 1970 [3]. Subsequently the study of $e^+e^- \to K^+K^-$ was conducted in experiments [4, 5, 6]. The most precise measurement of the cross section (10% statistical and 10% systematic uncertainties) was performed with the OLYA detector at the VEPP-2M collider [5, 7]. The urgency of the charged kaon form factor measurement is also motivated by a recent announcement [8] about the observation of a wide resonance structure in the K^+K^- invariant mass spectrum near 1.5 GeV in the decay $J/\psi \to K^+K^-\pi^0$.

In the present work we report the results of the measurement of the $e^+e^- \to K^+K^-$ cross section in experiments with the SND detector at the VEPP-2M collider in the center-of-mass energy range $\sqrt{s}$ from 1.04 to 1.38 GeV.

II. THE SND DETECTOR AND EXPERIMENT

In 1995–2000 experiments with the SND detector [9] were carried out at the VEPP-2M e^+e^- collider [10] in the energy range from 0.36 to 1.38 GeV. The basic part of the SND detector is the three-layer electromagnetic calorimeter consisting of 1632 NaI(Tl) crystals. The energy and angular resolutions of the calorimeter depend on photon energy: $\sigma_E/E(\%) = 4.2\%/\sqrt[4]{E(GeV)}$ and $\sigma_{\varphi,\theta} = 0.82^\circ/\sqrt{E(GeV)} \oplus 0.63^\circ$. Charged-particle tracking is provided by two coaxial cylindrical drift chambers. The angular resolution is 0.5° and 2° for the azimuthal and polar angles, respectively. Muon identification is provided by the muon system consisting of two layers of streamer tubes and a layer of plastic scintillation counters. The solid angle coverage of the SND detector is 90% of 4π.

In the present work the data of two scans taken in 1997 (from 0.98 to 1.38 GeV) and one scan taken in 1999 (from 1.04 to 1.34 GeV) are used. The integrated luminosity of these experiments measured using e^+e^- elastic scattering is 6.7 pb^{-1}. The energy spread at each energy point does not exceed 1 MeV and is taken into account in the data analysis.

III. EVENT SELECTION

To select events of the process

$$e^+e^- \to K^+K^-, \tag{1}$$

we require the presence of two collinear charged particles originating from the e^+e^- interaction point. A deviation from collinearity ($\Delta\varphi$) in the plane perpendicular to the beam direction is determined by multiple scattering in the detector material in front of the tracking system and depends on the kaon energy. The following conditions on this parameter were required:
$|\Delta\varphi| \leq 15^\circ$ for $\sqrt{s} < 1.08$ GeV,
$|\Delta\varphi| \leq 8^\circ$ for 1.08 GeV $\leq \sqrt{s} < 1.1$ GeV,
$|\Delta\varphi| \leq 5^\circ$ for $\sqrt{s} \geq 1.1$ GeV.
A deviation from collinearity ($\Delta\theta$) in the plane passing through the beam is additionally affected by radiation from the initial e^+e^- state. To limit the energy of radiated photons, the condition $|\Delta\theta| \leq 10^\circ$ was used. It was required for both tracks that $r_i \leq 0.3$ cm and $|z_i| \leq 10$ cm, where r_i is the minimum distance from the track to the beam axis and z_i is the coordinate of the particle production point along the beam axis. The number of neutral particles detected in the event was not limited.

Basic background processes satisfying the selection criteria are processes with two collinear particles in the final state:

$$e^+e^- \to \pi^+\pi^- \tag{2}$$

$$e^+e^- \to e^+e^- \tag{3}$$

$$e^+e^- \to \mu^+\mu^- \tag{4}$$

To suppress the background from the process (3), we required that the energy deposition of the charged particles in the calorimeter be less than 0.7 $\sqrt{s}$ and their polar angles θ_i be in the range $50^\circ < \theta_i < 130^\circ$. The substantial part of the background from the process (3) is caused by particle hittings into the dead calorimeter counters. Such events, whose fraction is about 2%, were excluded from the analysis.

To suppress background from the process (4) and reject the cosmic-ray background, a signal from the muon system was used. The requirement of the absence of this signal decreased the background from the process (4) by approximately 2 orders of magnitude.

With these criteria 136532 events were selected in the energy interval from 1.04 to 1.38 GeV.

IV. BACKGROUND PROCESSES

For the additional suppression of the background from the processes (2)–(4), we used a difference in the energy deposition profile in the calorimeter layers for particles of the signal and background processes. Efficient $K-\pi$ separation provided by the calorimeter is possible in the energy range under study because of the substantial difference between kaons and pions in the ionization losses and in the penetration depths. The special separation parameters were created with the aid of the neural network approach [11]. Monte-Carlo simulated events were used for the network training.

For each detected particle in the event parameters were created to separate kaons and pions $(kp1, kp2)$, kaons and electrons $(ke1, ke2)$, kaons and muons $(km1, km2)$, pions and muons of $(pm1, pm2)$, pions and electrons $(pe1, pe2)$. The separation parameters were obtained for each energy point in the experiment. Distributions of the separation parameters for the data and simulated events of the signal and background processes are shown in Fig.1 and 2 for the energy point $\sqrt{s}$=1.2 GeV. Particles are numbered according to the value of the energy deposition in the calorimeter, the first particle being the one with the greatest energy deposition. To obtain the data distribution for the first (second) particle of the particular process the tight cuts on the separation parameters of the second (first) particle were used.

For the selection of $e^+e^- \to K^+K^-$ events, the following restrictions on the separation parameters of the particles were used:

$$\begin{aligned} &kp1 < 0.5,\ kp2 < 0.5, \\ &ke1 < 0.5,\ ke2 < 0.5. \end{aligned} \tag{5}$$

The role of conditions (5) in the suppression of the background is demonstrated in Fig.3, where the polar angle distribution for data events is shown before and after applying the selection criteria (5). While without the selection cuts (5) the background exceeded the signal by a factor of more than three, with the selection cuts it was reduced to a few percent only.

After applying the conditions (5), the contribution from the background process (4) was found to be negligible (less than 0.1% of the number of selected K^+K^- events). The

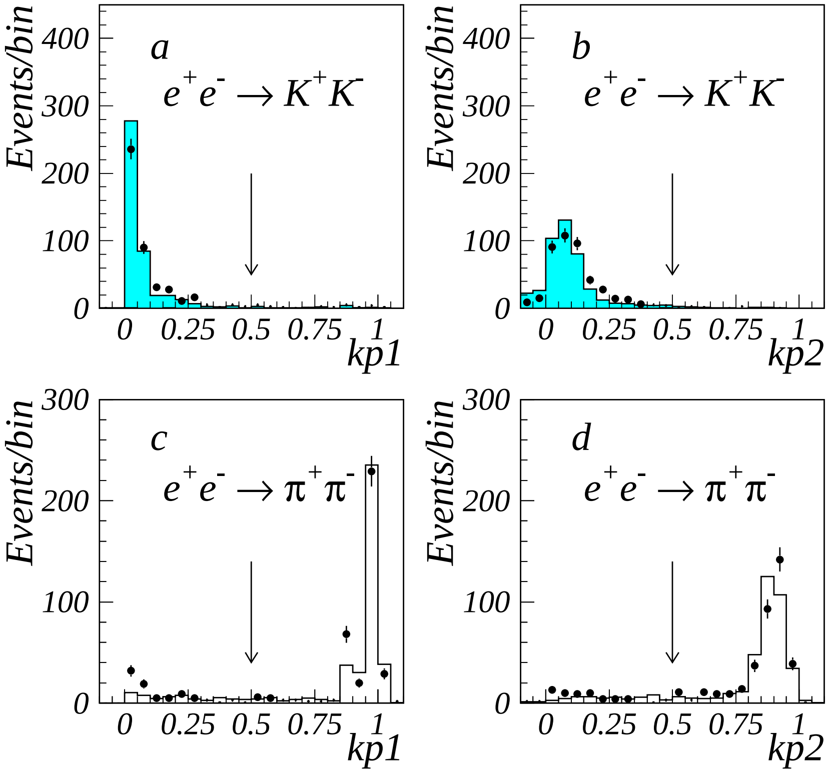

Figure 1: Distributions of the $K-\pi$ separation parameters for data (points with error bars) and simulated (histogram) events of the processes (1) and (2) for the energy point $\sqrt{s} = 1.2$ GeV. (a),(c) – the first particle, (b),(d) – the second particle. The cuts to select $e^+e^- \to K^+K^-$ events are indicated by arrows.

contributions of background processes (2) and (3) were determined from the simulation. Normalizing coefficients for the conversion of the number of events in simulation to the expected number of events in the data were determined in the following way. Using the tight conditions on the separation parameters, three classes of events were selected in which one of the processes (1)–(3) dominates. The numbers of data events in these classes (N^{KK}_{exp}, $N^{\pi\pi}_{exp}$ and N^{ee}_{exp}) are related to the numbers of simulated events of the processes $e^+e^- \to f$, $f = K^+K^-$, $\pi^+\pi^-$, e^+e^- assigned to the definite class ($N^{KK}_{mc,f}$, $N^{\pi\pi}_{mc,f}$ and $N^{ee}_{mc,f}$) in the

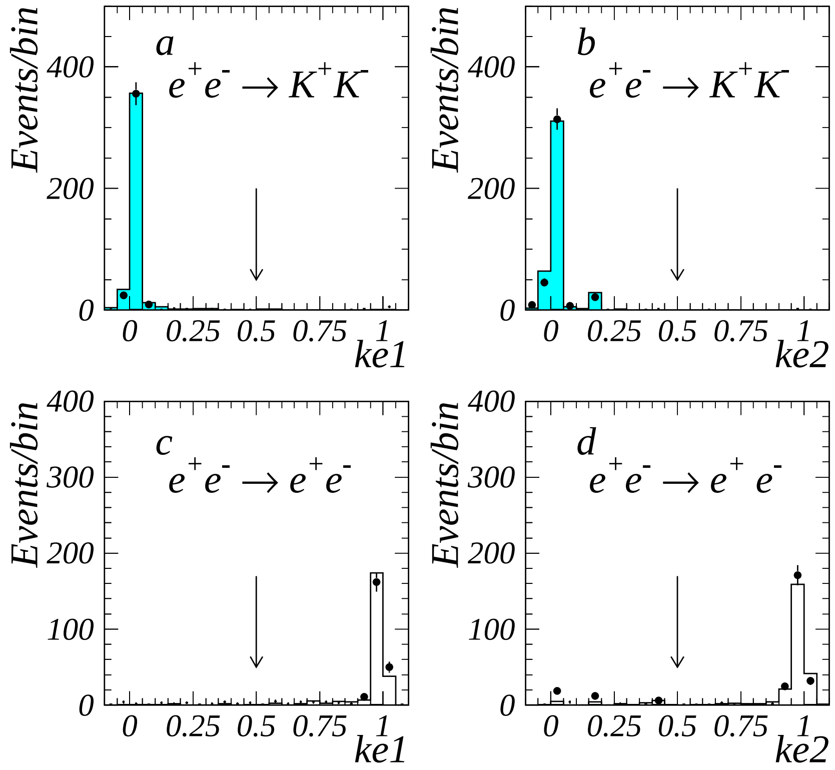

Figure 2: Distributions of the $K-e$ separation parameters for data (points with error bars) and simulated (histogram) events of the processes (1) and (3) for the energy point $\sqrt{s} = 1.2$ GeV. (a),(c) – the first particle, (b),(d) – the second particle. The cuts to select $e^+e^- \to K^+K^-$ events are indicated by arrows.

following way

$$\begin{aligned} N^{KK}_{exp} &= \sum_f N^{KK}_{mc,f} \cdot k_f, \\ N^{\pi\pi}_{exp} &= \sum_f N^{\pi\pi}_{mc,f} \cdot k_f, \\ N^{ee}_{exp} &= \sum_f N^{ee}_{mc,f} \cdot k_f, \end{aligned} \tag{6}$$

where k_f are normalizing coefficients to be found. A linear system of equations (6) allows to find coefficients $k_{K^+K^-}$, $k_{\pi^+\pi^-}$, $k_{e^+e^-}$ for each energy point. While determining N^{KK}_{exp}, $N^{\pi\pi}_{exp}$ and N^{ee}_{exp}, contributions from the beam and non-collinear backgrounds were taken into account and subtracted by the method described below. The origin of beam background is electron or positron collisions with residual gas in the accelerator beam pipe near the interaction point. Background from the process $e^+e^- \to \mu^+\mu^-$ in the pion class was sup-

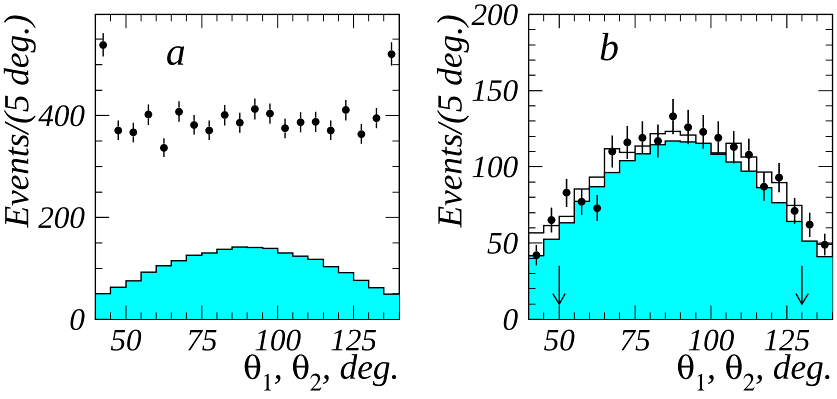

Figure 3: The polar angle distribution for data events (points with error bars) before (a) and after (b) applying the selection criteria (5). The shaded histogram shows the distribution for simulated $e^+e^- \to K^+K^-$ events. The hollow histogram is the sum of simulated distributions for the signal and background processes. Arrows indicate the selection boundaries on the angles θ_1, θ_2. Data are for the energy $\sqrt{s}$= 1.24 GeV.

pressed using the $\pi - \mu$ separation parameters. The obtained coefficients $k_{\pi^+\pi^-}$ and $k_{e^+e^-}$ were used for estimation of the pion and electron background in the event sample selected with standard criteria (5).

Besides processes with the collinear charged particles, other potential background sources are e^+e^- annihilation to three or more particles in the final state

$$\begin{aligned} &e^+e^- \to \pi^+\pi^-\pi^0\pi^0, \\ &e^+e^- \to \pi^+\pi^-\pi^+\pi^-, \\ &e^+e^- \to \pi^+\pi^-\pi^0, \end{aligned} \qquad (7)$$

and the beam related background.

The distributions of the event-vertex coordinate $z_0 = (z_1 + z_2)/2$ for the selected data events and simulated events of the processes (1)–(3) is shown in Fig.4(a) for the energy point $\sqrt{s}$=1.36 GeV. Most of the e^+e^- annihilation events are located in the range $|z_0| \leq 5$ cm. The beam background becomes significant in the region $|z_0| > 5$ cm. The distribution of the normalized energy deposition in the calorimeter $E_t/\sqrt{s}$ for the events with 5 cm $\leq |z_0| \leq$ 10 cm is shown in Fig.4(b). Events with $E_t/\sqrt{s} \leq 0.35$ are mainly from the beam background. They are uniformly distributed over $|z_0|$ while their distances from the track

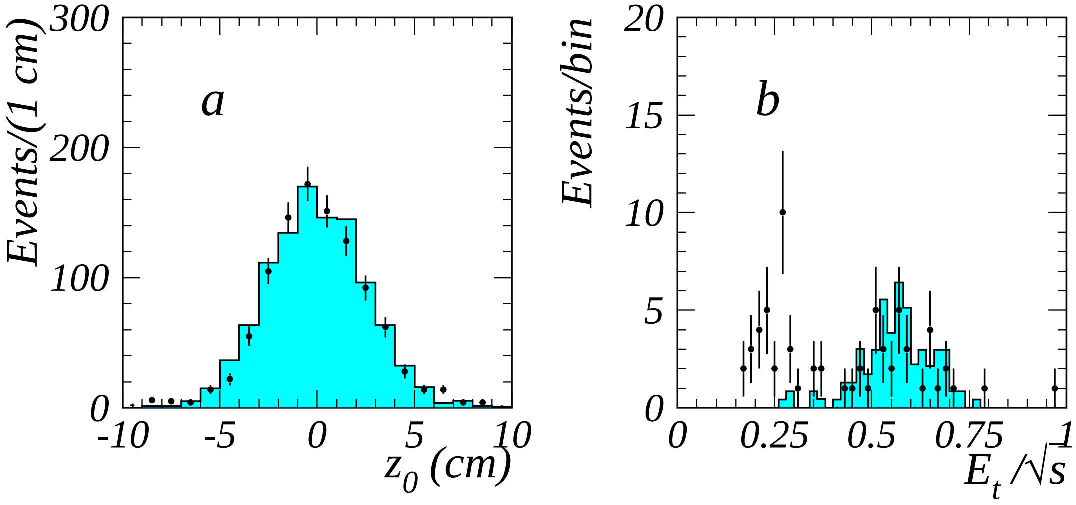

Figure 4: (a) Distribution of the event-vertex coordinate $z_0 = (z_1 + z_2)/2$ for selected data events (points with error bars) and simulated signal and background events (shaded histogram), $\sqrt{s}$=1.36 GeV. (b) Distribution of the normalized energy deposition in the calorimeter $E_t/\sqrt{s}$ for events with 5 cm $\leq |z_0| \leq$ 10 cm. Points with error bars represent the data. The shaded histogram is the simulation of the $e^+e^- \to K^+K^-$, $e^+e^- \to \pi^+\pi^-$, and $e^+e^- \to e^+e^-$.

to the beam axis are concentrated near zero. The contribution of the beam background to the selected data events was estimated as twice the number of events with 5 cm $\leq |z_0| \leq$ 10 cm and $E_t/\sqrt{s} \leq 0.35$ minus the calculated number of events of the processes (1)–(3).

The $\Delta\varphi$ distributions for selected data events and simulated events of the processes (1)–(3) and of the beam background are shown in Fig.5(a). The difference between the data and simulation distributions is shown in Fig. 5(b). It is seen that the remained background is uniformly distributed over the $\Delta\varphi$, as expected for the processes (7). The number of background events of the processes (7) was estimated as the number of events with $\Delta\varphi_0 < |\Delta\varphi| < 2\Delta\varphi_0$ minus expected number of events of the processes (1)–(3) and beam background. Here $\Delta\varphi_0$ equals 5°, 8° or 15° depending on the energy point.

Additional suppression of the background, both collinear and non-collinear, is provided by cuts on the ionization losses (normalized to those of the minimum ionizing particle) (dE/dx) in the drift chambers. The (dE/dx) distributions of the first particle for the data events of the processes $e^+e^- \to K^+K^-$, $e^+e^- \to \pi^+\pi^-$ and $e^+e^- \to e^+e^-$ are shown in

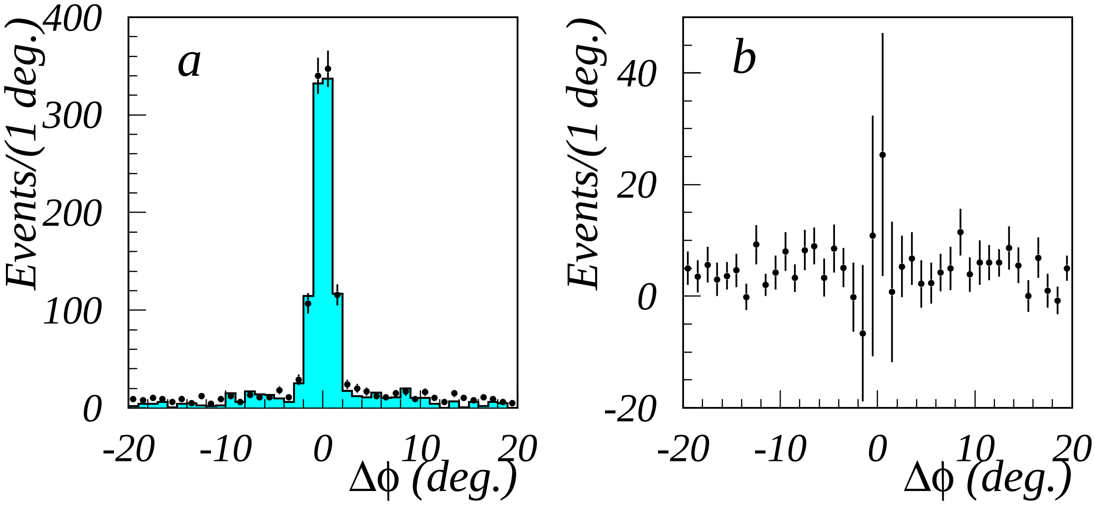

Figure 5: (a) The $\Delta\varphi$ distribution for selected data events (points with error bars). The shaded histogram shows the combined distribution for simulated events of the processes (1)–(3) and events of the beam background; $\sqrt{s}$=1.36 GeV. (b) The difference between the distributions shown in (a).

Fig. 6 for the energy points $\sqrt{s}$=1.08 GeV and 1.20 GeV. For events with $\sqrt{s} < 1.20$ GeV, we have used the following cuts on this parameter:

$\sqrt{s} \leq 1.11$ GeV: $(dE/dx)_1 > 2$;
$\sqrt{s} = 1.12 \div 1.18$ GeV: $(dE/dx)_1 > 1.5$;
$\sqrt{s} = 1.19 \div 1.20$ GeV: $(dE/dx)_1 > 1$.

The distributions of the normalized energy deposition in the calorimeter for data and simulated events at $\sqrt{s}$=1.36 GeV are shown in Fig.7. It is evident that at this energy the beam background can be efficiently eliminated by the condition $E_t/\sqrt{s} \geq 0.3$ without essential loss of efficiency to the process under study. This additional condition was used for the energy points with $\sqrt{s} \geq 1.22$ GeV.

After applying the above mentioned selection criteria and background subtraction, 54402 events of the process $e^+e^- \to K^+K^-$ were found. The numbers of events found for the signal (1) and background processes are presented in Table I for some energies. Errors in the number of kaons include uncertainties due to the statistical errors of the $k_{\pi^+\pi^-}$ and $k_{e^+e^-}$ coefficients and the subtraction of non-collinear and beam backgrounds. The contribution

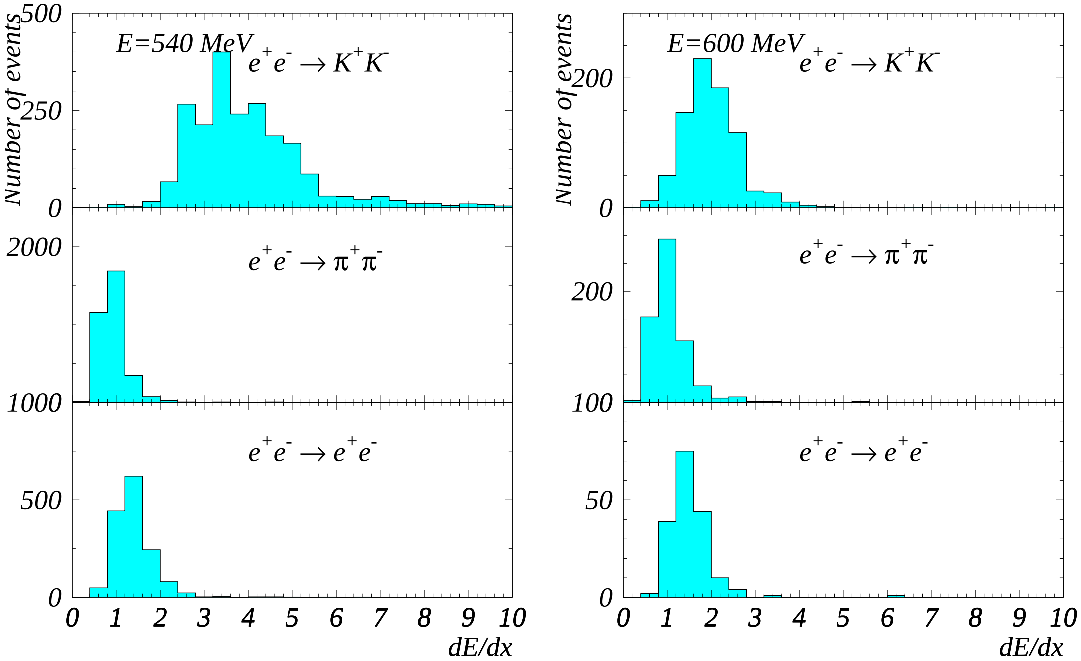

Figure 6: The distributions of the ionization losses $(dE/dx)_1$ of the first particle for data events of the processes $e^+e^- \to K^+K^-$, $e^+e^- \to \pi^+\pi^-$ and $e^+e^- \to e^+e^-$. (a) $\sqrt{s}$=1.08 GeV, (b) $\sqrt{s}$=1.20 GeV.

of background processes depends on energy and does not exceed 5% and 2% of the number of K^+K^- events for the processes (2) and (3), respectively. For beam background and background from the processes (7) it is less than 4% and 5%, respectively.

To estimate a possible systematic uncertainty due to subtraction of the $e^+e^- \to \pi^+\pi^-$ background we performed its independent estimation using the difference in the ionization losses of kaons and pions in the drift chambers (Fig. 6). For the 1999 energy scan, from the ratio of the number of events in the regions with $(dE/dx)_1 \leq 1$ and $(dE/dx)_1 > 1$ (or $(dE/dx)_2 \leq 1$ and $(dE/dx)_2 > 1$ for $\sqrt{s} < 1.20$ GeV) the number of background events $N(\pi^+\pi^-)$ was found to be 47 ± 30 for $\sqrt{s} \leq 1.20$ GeV, and 157 ± 29 for $\sqrt{s} > 1.20$ GeV. The corresponding numbers of pionic events, calculated according to the simulation using the procedure described earlier, are 58 ± 2 and 117 ± 6. Two methods of $e^+e^- \to \pi^+\pi^-$ background evaluation give the results which agree with each other. Nevertheless, the difference between the two calculations was used as an estimate of the accuracy of pionic

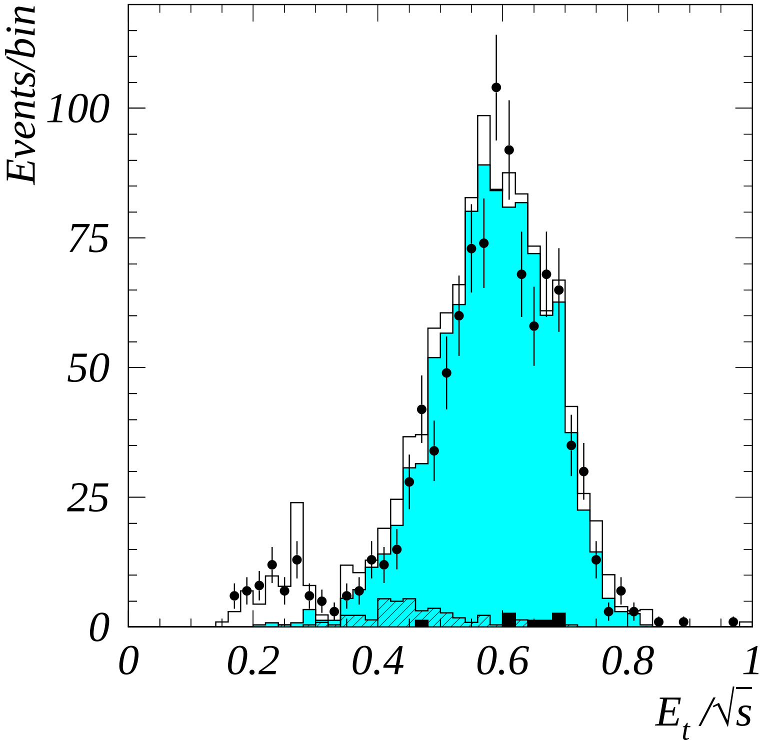

Figure 7: Distributions of the normalized energy deposition in the calorimeter $E_t/\sqrt{s}$ at $\sqrt{s}$=1.36 GeV. The shaded, hashed, and solid histograms are simulations of the processes $e^+e^- \to K^+K^-$, $e^+e^- \to \pi^+\pi^-$, and $e^+e^- \to e^+e^-$, respectively. The hollow histogram shows the total contribution from the process $e^+e^- \to K^+K^-$ and from all background processes including the beam background.

background determination. The corresponding systematic error in the number of events of the process $e^+e^- \to K^+K^-$ is 0.1% for $\sqrt{s} \leq 1.20$ GeV ($N(K^+K^-) = 11230$), and 1.4% for $\sqrt{s} > 1.20$ GeV ($N(K^+K^-) = 2900$).

The independent estimation of the background from electrons was performed by using the difference in the angular distributions for events of the $e^+e^- \to e^+e^-$ and the signal process. The ratio of the number of events in the regions with ($60° < \theta_i < 120°$) and ($50° \leq \theta_i < 60°$, $120° < \theta_i \leq 130°$) was used. Events with ($ke1 < 0.1$, $ke2 < 0.1$) were rejected to enhance sensitivity to electrons. This condition significantly reduces the number of K^+K^- events while the efficiency to the background process remains almost intact. The number of background events $N(e^+e^-)$ was found to be 35 ± 28 for $\sqrt{s} \leq 1.20$ GeV and

Table I: e^+e^- center-of-mass energy ($\sqrt{s}$), the number of selected $e^+e^- \to K^+K^-$ events ($N(K^+K^-)$) with subtracted background, calculated numbers of background events from $e^+e^- \to \pi^+\pi^-$ ($\bar{N}_{\pi^+\pi^-}$) and $e^+e^- \to e^+e^-$ ($\bar{N}_{e^+e^-}$), numbers of beam background events (N_1) and events of the e^+e^- annihilation into the final states with two non-collinear charged particles (N_2).

$\sqrt{s}$, GeV	$N(K^+K^-)$	$\bar{N}_{\pi^+\pi^-}$	$\bar{N}_{e^+e^-}$	N_1	N_2
1.04	1347.4 ± 38.5	0.1 ± 0.1	≤ 0.07	10.3 ± 6.8	10.2 ± 4.5
1.10	2042.0 ± 49.3	3.0 ± 1.3	≤ 0.9	31.5 ± 9.9	30.5 ± 8.1
1.15	281.7 ± 17.4	3.1 ± 2.4	0.3 ± 0.3	3.3 ± 0.5	4.0 ± 3.5
1.20	1600.2 ± 42.5	38.7 ± 2.3	≤ 1.1	28.3 ± 8.0	25.7 ± 7.4
1.25	697.7 ± 28.0	13.1 ± 2.5	5.3 ± 2.2	-	14.0 ± 4.9
1.30	792.9 ± 30.7	32.0 ± 2.3	7.6 ± 2.8	-	41.2 ± 7.3
1.35	718.7 ± 32.9	38.4 ± 14.3	9.0 ± 4.1	-	29.0 ± 7.9
1.38	1127.3 ± 36.0	41.3 ± 3.2	19.4 ± 4.7	-	28.1 ± 6.7

7 ± 24 for $\sqrt{s} > 1.20$ GeV. A calculation according to the simulation gives 3 and 17 events, respectively. The difference between two estimations, 0.3% of the number of K^+K^- events for the entire energy range, was used as a measure of the systematic uncertainty due to subtraction of the $e^+e^- \to e^+e^-$ background.

V. DETECTION EFFICIENCY

The detection efficiency for the process $e^+e^- \to K^+K^-$ was determined from Monte-Carlo simulation [12]. In the simulation the emission of photons by initial particles was taken into account [13, 14], and the detection efficiency was evaluated as a function of the center-of-mass energy $\sqrt{s}$ and the energy E_γ of the photon radiated by initial particles:

$$\varepsilon(\sqrt{s}, E_\gamma) = \varepsilon_0(\sqrt{s}) f(\sqrt{s}, E_\gamma), \tag{8}$$

where $\varepsilon_0(\sqrt{s})$ is the efficiency with no photon emission. The dependence of $f(\sqrt{s}, E_\gamma)$ on the photon energy at $\sqrt{s}$=1.12, 1.18, 1.24, and 1.36 GeV is shown in Fig.8.

The detection efficiency determined from simulation was multiplied by the correction

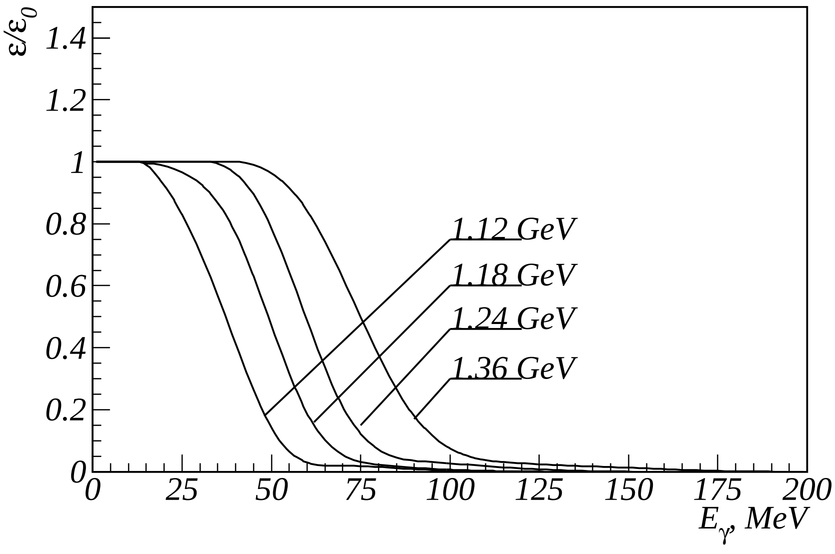

Figure 8: Detection efficiency of the process $e^+e^- \to K^+K^-$ versus the energy of the photon emitted by initial particles for $\sqrt{s}$=1.12, 1.18, 1.24 and 1.36 GeV.

factor, which takes into account the data-simulation difference in the detector response. The total correction factor is the product of correction factors related to specific selection condition. The correction factor for a given condition was calculated as

$$\delta_\varepsilon = \frac{N_{K^+K^-}(exp) \cdot N^{(1)}_{K^+K^-}(mc)}{N^{(1)}_{K^+K^-}(exp) \cdot N_{K^+K^-}(mc)}, \tag{9}$$

where $N_{K^+K^-}(exp)$, $N_{K^+K^-}(mc)$ are the numbers of K^+K^- events in the data and simulation, respectively, with the condition applied, $N^{(1)}_{K^+K^-}(exp)$, $N^{(1)}_{K^+K^-}(mc)$ are the numbers of events with the condition removed. To suppress the background, the conditions on other parameters were tightened and additional conditions on the ionization losses in the drift chambers were applied.

To obtain the correction related to the $\Delta\theta$ cut we used events with $|\Delta\theta| \leq 50°$. The distribution of $\Delta\theta$ is strongly influenced by the photon emission from the initial state. Therefore, the experimental dependence of the cross section on energy was implemented in the simulation of the $e^+e^- \to K^+K^-$ process. The correction factor for the cut $|\Delta\varphi| \leq \Delta\varphi_0$ was determined expanding the implied angular range by a factor of 2.

The correction factor obtained for different energy points is shown in Fig.9(a). The correction factor shown does not include the correction for the cuts (5), related to the particle separation parameters, which is given separately in Fig.9(b). The average accuracy of the

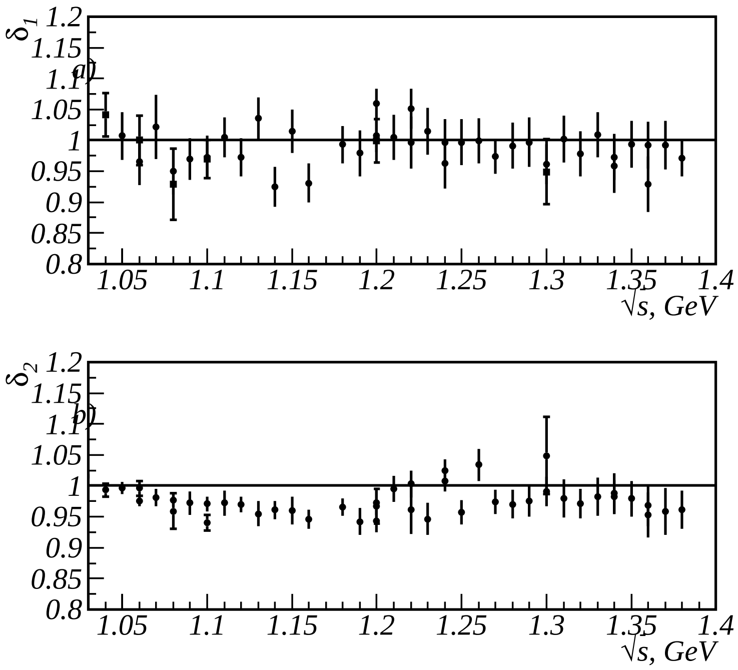

Figure 9: The efficiency correction factors for all selection conditions except the cuts (5) (a), for the cuts (5) on the particles separation parameters (b).

correction factor determination is 4.4%. The values of the corrected detection efficiencies $\varepsilon_0(\sqrt{s})$ are listed in Table II. The efficiency changes from 30% to 50% in the energy range under study.

VI. CROSS SECTION OF THE PROCESS $e^+e^- \to K^+K^-$

The visible cross section σ_{vis} for the process under study, directly observed in the experiment, is related to the Born cross section $\sigma_{K^+K^-}$ as follows

$$\sigma_{vis}(\sqrt{s}) = \int\limits_0^1 \sigma_{K^+K^-}(\sqrt{s(1-z)})F(s,z)\varepsilon(\sqrt{s},z)dz, \tag{10}$$

where $F(s,z)$ is a function describing a probability distribution of the energy fraction $z = 2E_\gamma/\sqrt{s}$ taken away by the additional photon with energy E_γ radiated from the initial state [13]. Formula (10) can be rewritten in the traditional form

$$\sigma_{vis}(\sqrt{s}) = \varepsilon_0(\sqrt{s})\sigma_{K^+K^-}(\sqrt{s})(1+\delta(\sqrt{s})), \tag{11}$$

where $\delta(\sqrt{s})$ is a radiative correction. The following procedure was used to extract the experimental values of the Born cross section. The visible cross section for the i-th energy point is equal to

$$\sigma_{vis,i} = \frac{N_{K^+K^-,i}}{IL_i}, \tag{12}$$

where $N_{K^+K^-,i}$ is the number of selected $e^+e^- \to K^+K^-$ events and IL_i is an integrated luminosity. The measured energy dependence of the visible cross section is approximated by a function calculated according to the formula (10) with the use of several models for the Born cross section. As a result of the approximation, the parameters of the model are determined and the following function is calculated

$$R(\sqrt{s}) = \frac{\sigma_{vis}(\sqrt{s})}{\sigma_{K^+K^-}(\sqrt{s})}. \tag{13}$$

Then the experimental Born cross section is determined through the formula

$$\sigma_{K^+K^-,i} = \frac{\sigma_{vis,i}}{R(\sqrt{s_i})}. \tag{14}$$

The model dependence of the result is estimated from its variation under different models for the Born cross section.

The Born cross section for the $e^+e^- \to K^+K^-$ was described by the model of Vector Meson Dominance [15, 16]:

$$\sigma_{K^+K^-}(\sqrt{s}) = \left|\sum_V A_V + \sum_{V'} A'_V\right|^2, \tag{15}$$

where $V = \rho, \omega, \phi$, $V' = \rho', \omega', \phi'$. The ρ, ω, ϕ mesons amplitudes were taken in the form:

$$\begin{aligned}
&A_V = \sqrt{12\pi \frac{m_V^3 B_{V\to e^+e^-}\Gamma_V \Gamma_{V\to K^+K^-}(s)}{s^{3/2}}} \cdot \frac{f_V}{D_V}, \\
&D_V(s) = m_V^2 - s - i\sqrt{s}\Gamma_V(s), \\
&\Gamma_V(s) = \sum_f \Gamma_{V\to f}(s), \quad \Gamma_{V\to f}(m_V^2) = \Gamma_V B_{V\to f}, \\
&\Gamma_{\rho\to K^+K^-}(s) = \Gamma_{\omega\to K^+K^-}(s) = 0.5 \cdot \Gamma_{\phi\to K^+K^-}(s),
\end{aligned} \tag{16}$$

where m_V, Γ_V are mass and total width of the resonance, $\Gamma_{V\to f}(s)$, $B_{V\to f}$ are partial width and the branching ratio of the V meson decay into the final state f, f_V is the phase factor. Energy dependence of the resonance width was calculated taking into account the main decay modes. The parameters of the ρ, ω and ϕ mesons were taken from [16].

The amplitudes for the excited states V' were written as follows:

$$A_{V'} = \sqrt{\sigma_{V'} \frac{W(s)}{W(m_{V'}^2)}} \frac{m_{V'}\Gamma_{V'}}{D_{V'}} f_{V'}, \tag{17}$$

where $\sigma_{V'}$ is the cross section of the process $e^+e^- \to V' \to K^+K^-$ at $s = m_{V'}^2$.

$$\begin{aligned} W(s) &= q^3(s)/s^{5/2}, \\ q(s) &= \frac{\sqrt{s}}{2}(1 - \frac{4m_K^2}{s})^{1/2}. \end{aligned} \tag{18}$$

For masses and widths of ω', ϕ', the PDG values [16] were used. The mass and width of the ρ', as well as $\sigma_{V'}$ and the relative phases $f_{V'}$ were free parameters of the approximation. The ϕ meson phase was varied in the limits $180° \pm 30°$ to estimate the model dependence of the results. Besides, the approximation which takes into account the ρ'' and ω'' meson contributions was performed. In this case the phase of the ϕ meson was fixed at 180°, while masses and widths of the excited states varied relative to the PDG data within their uncertainties. Depending on the model, χ^2/Nd varied in the limits of 1.0-1.14.

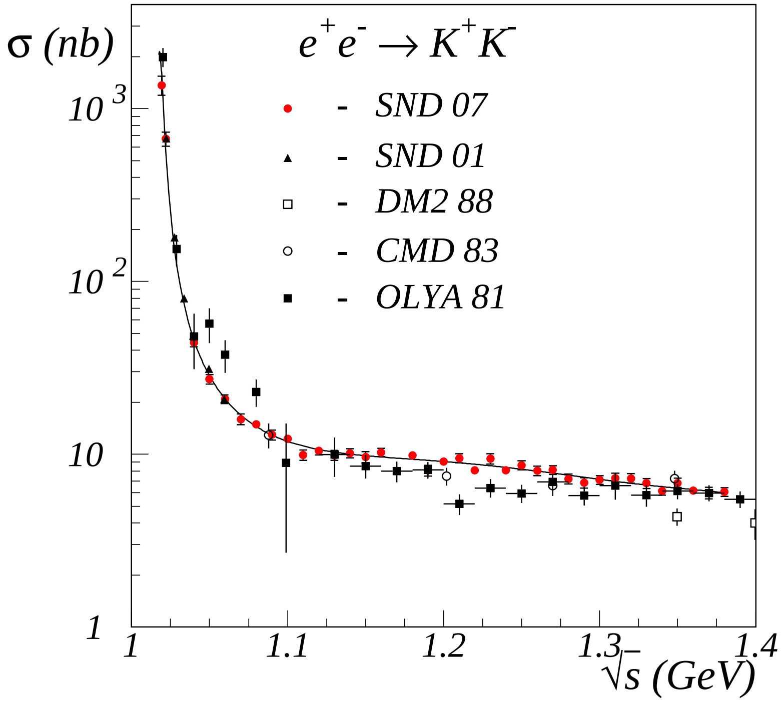

Figure 10: The total cross section for the process $e^+e^- \to K^+K^-$ in the energy range from 1.05 to 1.4 GeV obtained in different experiments. SND 07 – this work, SND 01 – [17], DM2 88 – [18], CMD 83 – [6]. OLYA 81 –[5]. The solid line shows the result of the approximation.

The obtained values of the Born cross section are shown in Figs. 10,11 and listed in Table II. The table also gives the values of the charged kaon form factor which is related to the

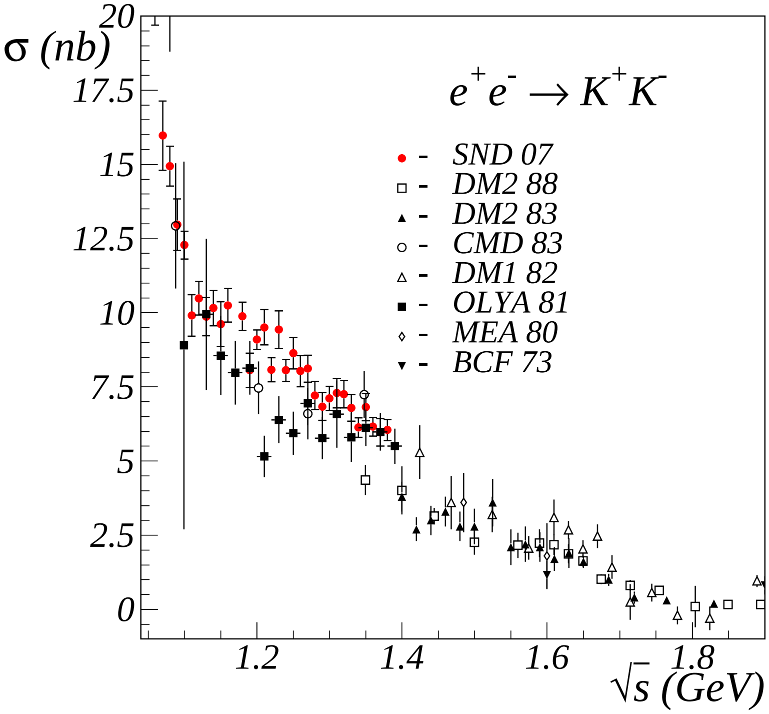

Figure 11: The $e^+e^- \to K^+K^-$ total cross section measured in different experiments in the energy range from 1.05 to 2 GeV. SND 07 – this work, DM2 88 – [18], DM2 83 – [20], CMD 83 – [6], DM1 81 – [19], OLYA 81 – [5], MEA 80 – [21], BCF 73 – [22].

Born cross section as follows

$$\begin{aligned} &\sigma_{K^+K^-}(\sqrt{s}) = \frac{\pi\alpha^2\beta^3}{3\cdot s}|F_{K^+}(\sqrt{s})|^2, \\ &\beta = \frac{2\cdot q(s)}{\sqrt{s}}. \end{aligned} \tag{19}$$

The radiative corrections calculated according to (11) are given as well. The average statistical error of the cross section measurement is equal to 4.4 %. An average systematic error is equal to 5.2% and includes inaccuracies in the determinations of the background (1.9%), detection efficiency (4.4%), luminosity (2%) and the model error (0.1%).

VII. DISCUSSION OF THE RESULTS

Results of the measurement of the $e^+e^- \to K^+K^-$ cross section $\sigma_{K^+K^-}(\sqrt{s})$ in the energy range $\sqrt{s}$ = 1.04–1.38 GeV, presented in this work, are the most precise at the present

Table II: The $e^+e^- \to K^+K^-$ cross section ($\sigma_{K^+K^-}$) and charged kaon form factor ($|F_{K^+K^-}|$) measured in this experiment. E is the center-of-mass energy, IL is an integrated luminosity, ε_0 is the detection efficiency, δ is a radiative correction, $N(K^+K^-)$ is the number of selected $e^+e^- \to K^+K^-$ events.

E, GeV	IL, nb^{-1}	ε_0	$(1+\delta)$	$N(K^+K^-)$	$\sigma_{K^+K^-}$, nb	$\lvert F_{K^+K^-}\rvert^2$
1.04	69.75	0.357 ± 0.013	1.252	$1347.4 \pm 36.7 \pm 12.3$	$44.30 \pm 1.66 \pm 1.88$	71.22 ± 4.08
1.05	83.91	0.389 ± 0.017	1.164	$1030.4 \pm 32.1 \pm 9.0$	$27.12 \pm 1.01 \pm 1.34$	34.96 ± 2.16
1.06	279.8	0.446 ± 0.014	1.076	$2832.3 \pm 53.2 \pm 21.7$	$20.90 \pm 0.45 \pm 0.70$	22.46 ± 0.91
1.07	97.74	0.426 ± 0.023	1.026	$682.0 \pm 26.1 \pm 8.2$	$15.96 \pm 0.64 \pm 0.96$	14.70 ± 1.07
1.08	550.47	0.427 ± 0.016	0.963	$3392.0 \pm 58.2 \pm 29.2$	$14.94 \pm 0.28 \pm 0.57$	12.06 ± 0.53
1.09	95.15	0.415 ± 0.017	0.901	$465.5 \pm 21.6 \pm 6.5$	$12.97 \pm 0.61 \pm 0.60$	9.34 ± 0.62
1.10	388.1	0.474 ± 0.012	0.905	$2042.0 \pm 45.2 \pm 20.6$	$12.28 \pm 0.27 \pm 0.37$	7.99 ± 0.30
1.11	91.66	0.480 ± 0.018	0.889	$387.0 \pm 19.7 \pm 2.5$	$9.91 \pm 0.51 \pm 0.47$	5.89 ± 0.41
1.12	231.26	0.511 ± 0.017	0.890	$1101.6 \pm 33.2 \pm 18.0$	$10.49 \pm 0.32 \pm 0.45$	5.76 ± 0.30
1.13	112.58	0.481 ± 0.019	0.884	$473.0 \pm 21.7 \pm 2.9$	$9.87 \pm 0.46 \pm 0.45$	5.05 ± 0.33
1.14	188.44	0.473 ± 0.018	0.887	$802.0 \pm 28.3 \pm 12.2$	$10.16 \pm 0.36 \pm 0.47$	4.87 ± 0.28
1.15	69.33	0.477 ± 0.020	0.888	$281.7 \pm 16.8 \pm 4.6$	$9.62 \pm 0.57 \pm 0.48$	4.35 ± 0.34
1.16	211.48	0.468 ± 0.017	0.889	$901.0 \pm 30.0 \pm 13.4$	$10.25 \pm 0.34 \pm 0.44$	4.39 ± 0.24
1.18	307.58	0.502 ± 0.017	0.891	$1358.4 \pm 36.9 \pm 14.8$	$9.88 \pm 0.27 \pm 0.38$	3.86 ± 0.18
1.19	172.29	0.444 ± 0.020	0.892	$548.9 \pm 23.4 \pm 8.1$	$8.05 \pm 0.34 \pm 0.45$	3.02 ± 0.21
1.20	397.6	0.497 ± 0.010	0.894	$1600.2 \pm 40.0 \pm 15.0$	$9.09 \pm 0.23 \pm 0.22$	3.28 ± 0.12
1.21	151.45	0.481 ± 0.020	0.897	$621.2 \pm 24.9 \pm 12.3$	$9.50 \pm 0.38 \pm 0.46$	3.32 ± 0.21
1.22	342.87	0.505 ± 0.019	0.898	$1248.5 \pm 35.3 \pm 21.8$	$8.07 \pm 0.23 \pm 0.32$	2.73 ± 0.14
1.23	140.75	0.444 ± 0.021	0.902	$530.6 \pm 23.0 \pm 12.0$	$9.43 \pm 0.41 \pm 0.49$	3.10 ± 0.21
1.24	377.74	0.481 ± 0.015	0.903	$1320.9 \pm 36.3 \pm 22.5$	$8.06 \pm 0.22 \pm 0.30$	2.58 ± 0.12
1.25	209.00	0.428 ± 0.018	0.903	$697.7 \pm 26.4 \pm 13.5$	$8.64 \pm 0.33 \pm 0.42$	2.69 ± 0.17
1.26	162.90	0.496 ± 0.022	0.908	$595.7 \pm 24.4 \pm 10.0$	$8.03 \pm 0.33 \pm 0.41$	2.45 ± 0.16
1.27	241.26	0.452 ± 0.016	0.907	$802.0 \pm 28.3 \pm 16.0$	$8.14 \pm 0.29 \pm 0.36$	2.43 ± 0.14
1.28	228.98	0.472 ± 0.021	0.908	$708.1 \pm 26.6 \pm 14.4$	$7.22 \pm 0.27 \pm 0.39$	2.11 ± 0.14
1.29	271.88	0.456 ± 0.022	0.909	$770.8 \pm 27.8 \pm 15.4$	$6.85 \pm 0.25 \pm 0.40$	1.97 ± 0.14
1.30	271.14	0.453 ± 0.017	0.909	$792.9 \pm 28.2 \pm 16.6$	$7.12 \pm 0.25 \pm 0.33$	2.01 ± 0.12
1.31	202.04	0.437 ± 0.021	0.910	$585.6 \pm 24.2 \pm 11.4$	$7.30 \pm 0.30 \pm 0.40$	2.03 ± 0.14
1.32	235.80	0.415 ± 0.019	0.910	$645.8 \pm 25.4 \pm 12.7$	$7.26 \pm 0.29 \pm 0.37$	1.99 ± 0.13
1.33	292.78	0.420 ± 0.020	0.914	$761.6 \pm 27.6 \pm 15.4$	$6.79 \pm 0.25 \pm 0.38$	1.84 ± 0.12
1.34	438.67	0.456 ± 0.017	0.915	$1121.8 \pm 33.5 \pm 23.5$	$6.13 \pm 0.18 \pm 0.28$	1.64 ± 0.09
1.35	256.66	0.450 ± 0.022	0.912	$718.7 \pm 26.8 \pm 21.5$	$6.82 \pm 0.26 \pm 0.39$	1.80 ± 0.12
1.36	625.16	0.432 ± 0.018	0.913	$1524.2 \pm 39.0 \pm 29.2$	$6.15 \pm 0.16 \pm 0.27$	1.61 ± 0.08
1.37	256.16	0.437 ± 0.024	0.914	$610.8 \pm 24.7 \pm 17.2$	$5.97 \pm 0.24 \pm 0.39$	1.55 ± 0.12
1.38	479.75	0.424 ± 0.019	0.917	$1127.3 \pm 33.6 \pm 20.5$	$6.05 \pm 0.18 \pm 0.31$	1.56 ± 0.09

time. The obtained measurement errors, both statistical and systematic, are 2 times less than achieved in the previous most precise experiment with the detector OLYA [5]. Some deviations of the measured cross section from the results of [5] are observed. In the energy range 1.05–1.08 GeV, the cross section obtained in [5] is approximately 60% higher than our results (2 standard deviations), while in the energy range 1.15–1.25 GeV the results of [5] lay systematically 25% lower than those obtained in this work (3 standard deviations). On the other hand, our results agree well with the previous SND measurements [17] in the energy range near the ϕ meson and with results of [6] (Fig.10).

VIII. CONCLUSION

In this work the cross section of the process $e^+e^- \to K^+K^-$, and the charged kaon electromagnetic form factor, was measured in the energy range $\sqrt{s} = 1.04$–1.38 GeV. The average statistical error of the measurement is 4.4%, the systematic error is 5.2%, which is approximately 2 times better than that achieved in the previous most precise experiment [5]. In general, the measured cross section is consistent with the results of the previous experiments, but has better accuracy.

We are grateful to S.Eidelman for his remarks and recommendations.

The work is supported in part by grants Sci.School-1335.2003.2, RFBR 04-02-16184-a, RFBR 04-02-16181-a, RFBR 05-02-161250-a, RFBR 06-02-16273-a, RFBR 07-02-00104-a.

---

[1] M.N. Achasov *et al.*, J. Exp. Theor. Phys. **1**03, 720 (2006), [Sov. Zh. Eksp. Teor. Fiz. **1**03, 831 (2006)].

[2] A.B. Clegg and A. Donnachie, Z. Phys. C **6**2, 455 (1994).
C. Bruch, A. Khodjamirian, J.H. Kuhn, Eur. Phys. J. C **39**, 41 (2005).

[3] V.E. Balakin *et al.*, Phys. Lett. B **41**, 205 (1972).

[4] G. Grosdidier *et al.*, Preprint LAL-80-35 (1980).

[5] P.M. Ivanov *et al.*, Phys. Lett. B **1**07, 297 (1981).

[6] L.M. Barkov *et al.*, Preprint NPI 83-85, Novosibirsk (1983).

[7] M.Yu. Lelchuk, PhD dissertation, Novosibirsk, 1982.

[8] M. Ablikim *et al.*, Phys. Rev. Lett. **9**7, 142002 (2006).

[9] M.N. Achasov *et al.*, Nucl. Instr. and. Meth. A **4**49, 125 (2000).

[10] A.N. Skrinsky, in Proceedings of the Workshop on Physics and Detectors for DAΦNE, Frascati, Italy, 1995, p.3.

[11] J.A. Anderson and E. Rosenfeld, Neurocomputing: Foundations of Research. The MIT Press. Cambridge MA 1988.
Bruce H. Denby, Comput. Phys. Commun. **4**9, 429 (1988).

[12] A.D. Bukin *et al.*, In Proc. of Workshop on Detector and Event Simulation in High Energy Physics, p.79-85, 8-12 April 1991, NIKHEFF, Amsterdam, Netherlands.

[13] E.A. Kuraev and V.S. Fadin, Yad. Fiz. **4**1, 733 (1985) [Sov. J. Nucl. Phys. **4**1, 466 (1985)].

[14] G. Bonneau and F. Martin, Nucl. Phys. B **4**1, 466 (1985).

[15] N.N. Achasov *et al.*, Yad. Fiz. **5**4, 1097 (1991), Sov.J.Nucl.Phys. **5**4, 664 (1991).
N.N. Achasov *et al.*, Int.J.of Mod.Phys. A **7** No.14, 3187 (1992).

[16] W.-M. Yao *et al.*, Review of Particle Physics, Journal of Physics G. Nuclear and Particle Physycs, **3**3, 1 (2006).

[17] M.N. Achasov *et al.*, Phys. Rev. D **6**3, 072002 (2001).

[18] D. Bisello *et al.*, Z. Phys. C **3**9, 13 (1988).

[19] B. Delcourt *et al.*, Phys. Lett. B **9**9, 257 (1981). J. Buon *et al.*, Phys. Lett. B **1**18, 221 (1982).

[20] J.E. Augustin *et al.*, LAL-83-21, Jul 1983. 31pp. Contributed to Int. Europhysics Conf. on High Energy Physics, Brighton, England, Jul 20-27, 1983.

[21] B. Esposito *et al.*, Phys. Lett. B **6**7, 239 (1977).
B. Esposito *et al.*, Lett. Nuovo Chim. **2**8, 337 (1980).

[22] M. Bernardini *et al.*, Phys. Lett. B **46**, 261 (1973).